

Casper: Accelerating Stencil Computation using Near-cache Processing

Alain Denzler¹ Rahul Bera¹ Nastaran Hajinazar^{1,2} Gagandeep Singh¹

Geraldo F. Oliveira¹ Juan Gómez-Luna¹ Onur Mutlu¹

¹ETH Zürich ²Simon Fraser University

ABSTRACT

Stencil computation is one of the most used kernels in a wide variety of scientific applications, ranging from large-scale weather prediction to solving partial differential equations. Stencil computations are characterized by three unique properties: (1) low arithmetic intensity, (2) limited temporal data reuse, and (3) regular and predictable data access pattern. As a result, stencil computations are typically bandwidth-bound workloads, which only experience limited benefits from the deep cache hierarchy of modern CPUs.

In this work, we propose Casper, a near-cache accelerator consisting of specialized stencil compute units connected to the last-level cache (LLC) of a traditional CPU. Casper is based on two key ideas: (1) avoiding the cost of moving rarely reused data through the cache hierarchy, and (2) exploiting the regularity of the data accesses and the inherent parallelism of the stencil computation to increase the overall performance. With minimal changes in LLC address decoding logic and data placement, Casper performs stencil computations at the peak bandwidth of the LLC. We show that, by tightly coupling lightweight stencil compute units near to LLC, Casper improves performance of stencil kernels by 1.65 \times on average, while reducing the energy consumption by 35% compared to a commercial high-performance multi-core processor. Moreover, Casper provides a 37 \times improvement in performance-per-area compared to a state-of-the-art GPU.

1 INTRODUCTION

A stencil operation [18] defines a computation pattern where elements in a multidimensional grid are updated based on the values of a fixed pattern of neighboring points. Computations using stencil operations (called *stencil computations*) are a key building block of important HPC applications [11] and are used in a wide range of scientific simulations, including climate modeling [16], seismic imaging [25], fluid dynamics, and electromagnetic simulations [40]. Stencil computations encompass a large percentage of the overall runtime of such applications [17, 23, 29]. For example, stencil computation represents over 90% and 60% of the overall runtime in computational fluid dynamics solver and COSMO climate simulation model, respectively. However, the current compute-centric processing systems, such as multi-core CPUs and GPUs, fail to fully utilize their on-chip resources (e.g., deep cache hierarchy, high throughput floating-point engines) when computing stencil operations. This results in lower performance and decreased energy efficiency for stencil computations in current systems.

Figure 1 shows the roofline plot [46] of important stencil kernels on a server-class CPU. The horizontal line demonstrates the peak floating-point performance of the system. The DRAM and LLC lines show the peak memory and LLC bandwidth, respectively. We make

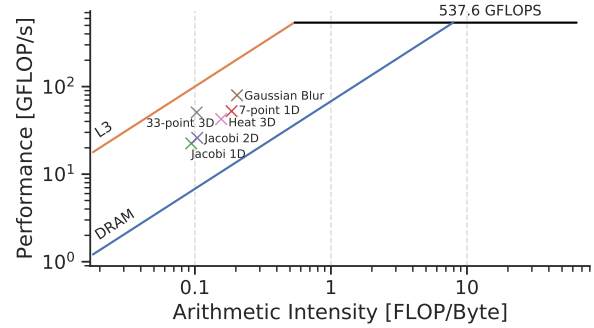


Figure 1: Roofline plot for a multi-core system running six stencil kernels.

two observations. First, the stencil kernels are *not compute bound*, having low arithmetic intensity ranging from 0.09 to 0.2 FLOP/Byte. Second, all the kernels are *bounded by memory resources*, i.e., located on the left side of the inflection point and below the memory lines. More importantly, all the kernels are located below the L3 line and above the DRAM line, which shows that the stencils are bound by the LLC bandwidth rather than the main memory. Given these observations, we conclude that the high number of LLC accesses is the main bottleneck for stencil computations, resulting in such computations to experience only limited benefits from the deep cache hierarchies in modern CPU architectures.

Prior works [4, 12, 30] also show that stencil kernels are bottlenecked by memory due to their low arithmetic intensity, leading to under-utilization of computational resources in compute-centric platforms (i.e., CPU, GPU). These prior works demonstrate that stencil kernels can only leverage 21.8% [4] and 46% [12] of the computational resources of a multi-core CPU and GPU, respectively, even in presence of code optimizations (e.g., temporal blocking). Therefore, general-purpose processors cannot deliver high performance and high efficiency (in terms of utilization) for stencil computations, thus opening up the space for custom stencil-based accelerators [33, 36].

Near-memory processing is a promising paradigm that aims to accelerate memory-bandwidth-bound workloads with low arithmetic intensity. [1, 15, 20, 22, 34, 34]. The key idea of the NMC paradigm is to move computation close to (i.e., near-memory) or even into (i.e., in-memory) the memory devices (i.e., caches, DRAM, storage) where the data resides, eliminating the need to move the data to the processor and resulting in increased performance and reduced energy consumption. Stencil computations are a prime candidate for acceleration using NMC paradigm. In this work, we explore the opportunity to improve the performance and energy efficiency of stencil computations in traditional multi-core CPUs by computing near LLC.

Why near LLC? We exploit LLC as the prime location for computations, as opposed to offloading the computation to the off-chip main-memory [22] or higher levels of caches (e.g., L2) for three main reasons. First, the per-thread dataset for stencil kernels in widely-deployed workloads are normally tiled to fit inside the LLC of traditional workstation-class CPUs [16, 41]. Hence, placing computation near LLC minimizes unnecessary data transfers, which eventually provides both higher performance and higher energy efficiency than computing inside core or main memory. Second, the on-chip LLC bandwidth is multi-fold higher than a traditional DDR-based DRAM main-memory bandwidth. Even compared to a high-bandwidth yet costly HBM interface, the on-chip LLC bandwidth can be readily exploited in any commodity off-the-shelf processor. Third, though computing in high-level caches (e.g., L2) can provide higher per-compute bandwidth on paper, moving data back and forth from LLC to higher-level caches reduces the effective bandwidth due to cache-protocol-induced additional transactions (e.g., back invalidations, write backs, etc.). Moreover, pulling data that provides low reuse (common in stencil computation data) to higher-level caches results in energy waste.

Thus **our goal** in this paper is to design a near-LCC accelerator that improves the performance and energy efficiency of stencil computations by minimizing the unnecessary data movement.

To this end, we propose Casper, a novel hardware/software code-sign specifically targeted at stencil computations. We minimize data movement by placing a set of pLSPU near the LLC of a traditional CPU architecture and provide novel mechanisms to introduce data mapping changes and support unaligned loads needed for high-performance stencil computations. Computation is mapped to pLSPU so that each SPU operates on the data that is located in the closest LLC slice. This reduces the overall data access latency and energy consumption while matching the compute performance to the peak bandwidth of the LLC.

Placing a stencil accelerator next to the LLC of a CPU introduces two key challenges. The first challenge is to maximize bandwidth utilization. A superscalar out-of-order CPU leverages its front-end structures such as reorder buffers and large instruction windows to exploit instruction-level parallelism, thus enabling high memory bandwidth utilization. To address this challenge, Casper introduces the notion of *stream* to expose the memory level parallelism that exists in the stencil computation to the SPUs. Each stream represents a set of consecutive memory accesses with a fixed stride. Knowing the stride for each stream, Casper can issue the memory accesses of the stream in parallel. The notion of stream enables Casper to maximize memory bandwidth utilization without requiring complex structures such as reorder buffers.

The second challenge is to minimize the data movement between different cache slices. In stencil computations, the neighboring grid points need to be accessed to compute the stencil operation for each grid point. However, current systems employ an address mapping scheme that distributes data over different LLC slices and provides load balance and fairness across CPU cores. Such a mapping scheme can potentially map neighboring grid points to different LLC slices, introducing data transfers over the NoC and thereby eliminating the benefits of near-cache computing. To address this challenge, Casper includes hardware support to align the data mapping to the

grid structure of the stencil computation and place neighboring grid points into the same slice of the LLC.

We evaluate Casper using six widely used stencil kernels with up-to 3-dimensional grid domains. Casper outperforms a commercial multi-core CPU on average by (up-to) 1.65 \times (4.16 \times) and reduces the energy consumption by 35%. Compared to a state-of-the-art GPU, Casper improves performance-per-area by 37 \times on average.

We make the following contributions:

- We propose Casper, a high-performance near-cache accelerator for stencil computations. Casper addresses the memory bottleneck in stencil computations by (1) minimizes the movement of data within the cache hierarchy, and (2) maximizing the utilization of the LLC bandwidth.
- We provide hardware support to change the mapping of cache lines to LLC slices to improve spatial data locality for stencil computations.
- We design an *efficient* mechanism to support unaligned loads directly from the LLC.
- We evaluate the effectiveness of Casper on six widely used stencil kernels and demonstrate that Casper improves performance and reduces the energy consumption by 1.65 \times and 35% on average compared to a commercial multi-core CPU.

2 BACKGROUND: STENCIL COMPUTATION

Stencil computations [18] update points in a data grid based on a fixed pattern of neighboring points. This fixed pattern, called the *stencil*, is applied on the complete grid iteratively until either a convergence criterion or a fixed number of time steps are reached. Stencil computations are widespread in scientific computing, and are considered one of the 13 dwarfs of scientific computing [11].

Stencil computations exhibit several common properties. We explain these properties using the *Jacobi* stencil as an example [14] which is commonly used to solve discretized partial differential equations. Figure 2 shows the source code and data access pattern of a 2-dimensional Jacobi stencil. The computation performs arithmetic mean of each point in the grid and its immediate neighbors in all directions. This implementation uses three nested loops where the outermost loop iterates over time steps and the two inner loops sweep over the complete 2D grid.

```
for (int t = 0; t < T; t++) {
    for (int i = 1; i < N-1; i++) {
        for (int j = 1; j < N-1; j++) {
            B[i][j] = 0.2 * (A[i][j]
                + A[i][j-1]
                + A[i][j+1]
                + A[i-1][j]
                + A[i+1][j]);
        }
    }
    // swap pointers
    temp = A; A = B; B = temp;
}
```

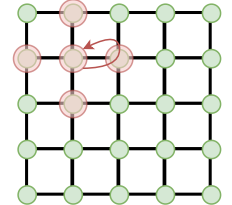


Figure 2: 2D Jacobi stencil pseudo-code and data access pattern.

From this example, we can identify four common properties of stencil computations. First, the computation is embarrassingly parallel because the read and write data sets are disjoint. Second,

the computation is regular and statically analyzable. The data dependencies and the structure of the computation can be analyzed ahead-of-time and do not depend on dynamic input. Third, the arithmetic intensity of the stencil is low. Fourth, only a few types of operations are needed to compute the stencil. For example, in case of *Jacobi* stencil, only a floating-point MAC operation is performed for each input grid point. These properties enable the opportunity for high-performance stencil acceleration since they provide well-balanced parallelism and predictable and uniform access patterns. Additionally, being memory-bound (Figure 1) makes stencils good candidates for near-memory acceleration.

In this work, we focus on stencil computations that apply *one* stencil to the complete dataset per time step. Related work on stencil computations, such as [18, 36] focuses on compound stencils, which apply *several* stencils using multiple input and intermediate arrays during each time step. These compound stencils are limited by DRAM bandwidth [36]. While both types of stencils are common in real-world workloads [10, 18], we focus on the first type which only applies one stencil per iteration.

3 CASPER: OVERALL ARCHITECTURE

3.1 Overview

The key idea of Casper is to place specialized stencil processing units (SPU) near the last-level cache (LLC) of a traditional CPU. As a typical LLC is partitioned into multiple cache slices, Casper places one SPU in each LLC slice. At a high level, each SPU performs the stencil operation on each grid point sequentially. The input grid points are accessed in row-major order, following their layout in memory. For each input grid point, the SPU loads the data from LLC either from the local or remote LLC slice. Once the data arrives at the SPU, the SPU’s execution unit performs a single multiply operation with a predefined constant, whose output is added to the accumulator. The final accumulated result is stored back into the output grid point only when all computations for the output grid point have been completed.

To accelerate the accesses to input grid points, Casper abstracts a series of data accesses using a *stream*. A *stream* is a sequence of data elements of the same type located in consecutive physical memory addresses [21]. A stream is represented by the start address, the data type width, number of elements, and a position pointer. Initially, the position pointer of a stream points to the start address. Upon receiving a control signal, the position pointer is advanced till the final element in the stream. The stream abstraction facilitates quick iteration over the data instead of loading each data element using absolute memory addresses. Since a stencil computation moves through a grid at the same pace maintaining the same relative offsets for the stencil pattern, SPU uses stream abstraction to accelerate input grid access. This allows the same stencil code to be reused for all the grid points, and multiple disjoint data sources to be easily included in the stencil pattern by referring to different streams.

3.2 Stencil Processing Unit

Figure 3 shows the architecture of a SPU. The main building blocks are (1) the instruction buffer, (2) the load queue, (3) the stream buffer, (4) the constant buffer, and (5) the execution unit. The complete SPU is pipelined to maintain single-cycle instruction throughput.

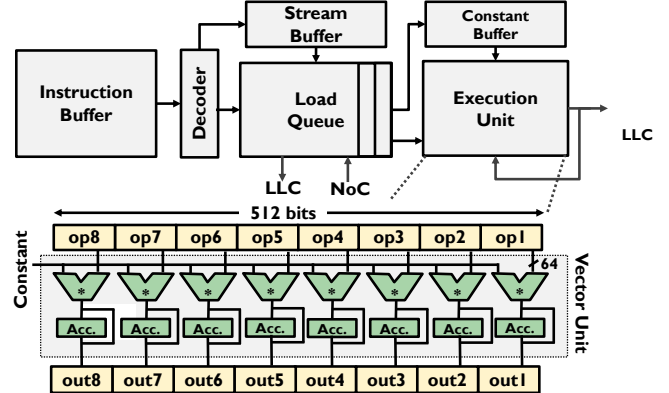


Figure 3: Components of one SPU.

The SPU controls the complete computation, from instruction fetch until retire. Therefore it does not involve any interaction with the CPU.

Instruction Buffer. The instruction buffer has a capacity to hold 64 *compressed* instructions to compute a stencil. Every instruction encodes the operands and the control signals for one type of stencil operation. The same sequence of instructions is applied to every stencil output grid point due to the regular nature of the stencil computation. We introduce the instruction set in Section 5.

Load Queue. The load queue is responsible for issuing data requests to the memory subsystem. While the SPU processes instructions in-order, the varying memory access latency can result in responses that arrive out-of-order. The load queue acts as a buffer to hold the data until all the previous, longer-latency memory requests have been completed. This buffer space ensures that the instruction order is maintained.

Stream and Constant Buffers. The stream buffer holds the current state of the streams. For every decoded instruction, this state is loaded from the buffer, and the effective address is calculated to issue the memory requests to LLC. The constant buffer holds the constant factors needed for the MAC operation. The stream and constant buffers are initialized by API calls before the SPU starts the stencil computation.

Execution Unit. As shown in Figure 3, the execution unit of a SPU is comprised of a 512-bit vector unit which operates on vectors of 8 double-precision floating-point elements. For every input grid point, the SPU loads the data elements from the neighboring points, multiplies them with a constant factor, and accumulates the results. This final accumulated result is then stored in the output grid point. Therefore, each SPU execution unit only computes one kind of instruction: a double-precision floating-point multiply-accumulate operation (MAC).

4 CASPER: MICRO-ARCHITECTURAL SUPPORT

4.1 Support to Unaligned Loads

While the stream abstraction offers efficient memory accesses, the LLC architecture only supports data accesses aligned to 64-byte boundaries. As the relative offsets used in streams are not necessarily aligned to 64-byte cacheline boundary, the loaded data might

need to be realigned before it can be used by MAC compute. For example, in Figure 4 each SPU computes 8 64-bit output grid points ($B[i]$) for a 3-point Jacobi-1D stencil. The access to the center point of the stencil $A[i]$ is correctly aligned to the 64-byte boundary (shaded in yellow) such that the data for this point can be used for computation as soon as it arrives at the SPU. However, to gather several input grid points at indices $+3$ ($A[i+3]$) and -3 ($A[i-3]$), the data coming from the cache needs to be correctly shifted (shaded in orange and red), and two cache lines need to be combined to assemble the operands for the computation. As a result, preparing the operand for the MAC unit involves two loads, one shift, and one combine operation on the data from the two cachelines. These additional operations due to unaligned data accesses not only drops the utilization of MAC units (e.g., the MAC utilization in Figure 4 drops from 4 load/store operations per 3 MACs to 5 load/store operations per 3 MACs), but also wastes precious cache bandwidth to load the data. To address the above challenge, we introduce two simple modifications to the LLC row decoding logic: (1) support to loading data aligned to any 8-byte boundary, and (2) support to correctly align data for SPU execution. Our modified LLC row decoding logic reduces SPU's complexity and area footprint since by only modifying the row decoding circuitry, we avoid the need for additional logic to shift and pack the partial cache lines, and/or a large register file inside SPU.

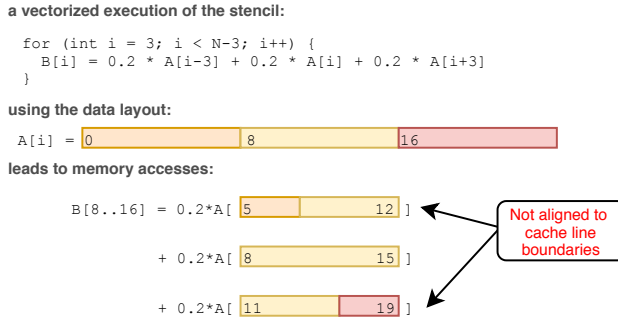


Figure 4: Unaligned loads occurring during the vectorized execution of a stencil.

Implementation Challenges. Loading data aligned to 8B boundaries potentially implies loading data located on two cache lines. This introduces two key challenges. First, two tags need to be matched to locate the two cache lines. Second, the correct data from both cache lines must be loaded using only one supplied address.

To address the first challenge, we enable the cache to match the two tags in parallel by adding a second read port to the tag array. Since the two cache lines involved in an unaligned load are always at consecutive addresses, they are guaranteed to be mapped to different cache sets, and thus, there are no conflicts during the tag matching process. If one or both cache lines are not in a readable state, a regular cache miss is generated, and the request is stalled until the miss is resolved.

To address the second challenge, we make changes into the LLC row decoding logic to load data either from the requested address or one of the cache lines located inside the 64B-vicinity of the

requested address. More specifically, we add one 3-to-1 multiplexer for each LLC SRAM row. The inputs to the multiplexer are set to the row decoder output of the current row and both the adjacent rows. The multiplexer selects the appropriate row(s) based on the row selection signal.

Loading Shifted Cache Lines. Figure 5 shows the execution sequence of unaligned access to the LLC. In this example, we consider the request to cache line holding elements 8 to 15, shifted to the right by three positions. This corresponds to the access to input grid points $A[i-3]$ in Figure 4. Let us first consider the case where the two cache lines involved in the access are mapped to the *same* cache way. One cache way consists of $4 \times 32\text{kB}$ data arrays, each having $2 \times 16\text{kB}$ subarrays. One 16kB subarray holds 64 consecutive bits of a cache line for all the 2048 sets. Thus, each 64-bit segment of a cache line is stored in a different SRAM subarray.

As shown in Figure 5, all the elements required to build the 64B block of data are stored in different subarrays of a single cache way (orange and green elements on the left part of the figure). Therefore, by selecting the correct data at the subarray level (using shift direction and amount) it is possible to load all the elements using only one command, while maintaining the same throughput and latency as a regularly aligned load. To complete the unaligned access, we need to rotate the data such that the correct element is at the first position of the 64B block of response data. To accomplish this, we use a rotate network that performs this operation before the final output. In this way, the SPU can load data from the LLC aligned to arbitrary 8B boundaries.

If the two cache lines involved in an unaligned load are mapped to *different* ways, the load sequence is similar. As the data and tag access happen in parallel inside the cache, the data load is initiated on all cache ways before the way hit has been confirmed. Thus for any access, all the ways present the data for the requested set on their output bus. Based on the way hit, the data from the correct way is selected for the output. We modify the way hit selection to select each subarray's output independently, depending on the shift amount and direction supplied with the request.

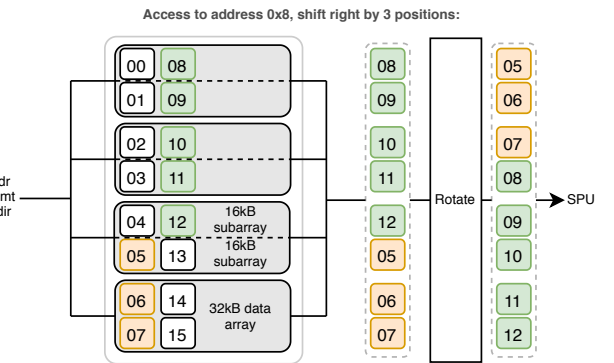


Figure 5: Loading unaligned data from the LLC. The two cache lines involved in the access are mapped to the same cache way. One cache way consists of $4 \times 32\text{kB}$ data arrays, each having $2 \times 16\text{kB}$ subarrays.

4.2 LLC Data Mapping

Computing at the LLC’s peak throughput is only possible if all the plSPU in the system load data from their closest LLC slice, thus avoiding the network-on-chip (NoC) traffic overhead. However, the existing mapping of memory addresses to the LLC slices does not guarantee mapping consecutive cache lines to the same slice to provide better fairness and load balancing [47]. Due to the streaming nature of the stencil computation and the dependency on a small neighborhood of grid points, scattering data through the cache slices would increase the number of remote data requests per SPU, penalizing performance and energy consumption. Thus Casper maps blocks of consecutive memory addresses to the same LLC slice. To achieve this, we introduce hardware support for *stencil segments* [6]. A stencil segment is a physically contiguous block of memory that is exposed by the system to hold stencil data. Casper identifies a stencil segment and changes the segment mapping to LLC slices such that physically contiguous blocks of data are mapped to the same slice. At each NoC injection point, the system checks if the address is part of the stencil segment, and, if valid, applies a new hash function (i.e., a linear hash that statically maps contiguous blocks of 128kB to LLC slices in round-robin fashion) to route a memory request. Otherwise, the existing hash is applied. By deciding which mapping function to use based on a memory request’s physical address, each address is mapped to precisely one cache slice, regardless of whether it contains stencil data or not.

4.3 Coherence Support

A SPU loads data from the LLC by directly injecting a load/store request in the LLC controller’s request queues. Casper does not impact the current cache coherency mechanism, because requests from the SPU are injected into the same request queues as conventional requests from the CPU cores and the private caches. If a write request from an SPU targets a cache line that is not in writable state in the LLC, the coherency mechanism will trigger necessary state transitions and invalidations to allow the write to complete.

4.4 Concurrent Execution with CPU and Context Switching

To enable concurrent execution with the CPU, we reserve one way of the LLC for other applications running in the CPU, similar to prior work [15]. Additionally, high priority is assigned to the SPU process to minimize the occurrence of context switches. If a context switch happens, the state of the SPU remains unchanged, because it is not allowed to start a new stencil computation before the current computation finishes.

5 CASPER: PROGRAMMING MODEL SUPPORT

5.1 Casper ISA

Casper makes use of specialized instructions to compute each point involved in the stencil operation. Every Casper instruction is 15-bits wide and comprises of (1) 4b constant buffer index, (2) 4b stream buffer index, (3) 1b shift direction, (4) 3b shift amount, and (5) 3b control bits. Note that Casper reuses the instructions for all the grid points, thus reducing instruction count.

After decoding a new instruction, the SPU uses constant index to load the double-precision constant value from the constant buffer. The stream index is used to point the stream buffer to gather memory address of the requested stream. The shift direction and the shift amount are used to initiate appropriate load request to the LLC. Three control bits, *clear accumulator*, *enable output*, and *advance stream* are used to reset the accumulators in the execution unit, enable the contents of the accumulator to be stored into the results array, and to advance the stream pointers, respectively. We also provide a programming library that allows the user to easily generate Casper instructions from user-level code.

5.2 Casper API

Table 1 shows Casper API functions. Calls to API functions are mapped directly to ISA instructions, which are broadcasted to all SPUs. These instructions are integrated into the existing ISA using spare instruction opcodes.

6 AN EXAMPLE: JACOBI-2D STENCIL

We illustrate how to program Casper using the code in Figure 6 as an example. The code implements the Jacobi-2D stencil presented in Section 2. We explain the example using a system consisting of 4 LLC slices and plSPU.

```

1 void computeStencil(void* code) {
2
3     /* stencil segment holding 4MB */
4     uint64_t segment = initializeStencilSegment(4194304);
5
6     double* A = (double*) segment;
7     /* results start halfway through segment */
8     double* B = (double*) segment + 2097152;
9
10    /* initialize data ... */
11
12    initConstant(0.2, 0);
13
14    initStencilcode(code, 5);
15
16    /* 128kB block holds 16384 doubles */
17    int blockSize = 16384;
18
19    /* rows of 128 elements */
20    int rowLength = 128;
21
22    for (int i = 0; i < 4; i++) {
23        initStream(&A[i*blockSize-rowLength], 1, i);
24        initStream(&A[i*blockSize], 2, i);
25        initStream(&A[i*blockSize+rowLength], 3, i);
26        initStream(&B[i*blockSize], 0, i);
27        /* 512kB is 65536 doubles */
28        setNElements(65536, i);
29    }
30    startAccelerator();
31}

```

Figure 6: Program code for Jacobi 2D stencil.

First, a stencil segment covering 4MB is allocated (line 4). Then, we define the start of the arrays A and B such that the same grid point of both arrays is mapped to the same LLC slice (lines 6-8). The programmer then initializes the arrays with the stencil data. Furthermore, the constant for the multiplication (line 12) and the stencil instructions (line 14) are sent to the plSPU. The streams for all the plSPU are configured inside the loop (lines 22-29). In this example, four streams are configured: three input streams to load the elements at A[j-1][i], A[j][i] and A[j+1][i] (lines 23-25),

Table 1: Casper Programmer API

Function	Parameters	Description
<code>initStencilSegment</code>	int size	Requests a physically contiguous memory region of the specified size from the system to hold the stencil data
<code>initStencilcode</code>	addr A, int length	Takes a pointer to the microcode and the length of the code. After generating the code with helper functions provided by the programming library, the code is then broadcast to the plSPU
<code>initConstant</code>	double const, int index	Initializes constant values that will be used during the multiplication step of a stencil operation. The function sets the specified constant value at the given index in the constant buffer
<code>initStream</code>	addr A, int streamID, int accID	Configures the streams used in the stencil code. The streams are configured per SPU to enable the programmer to tune the data layout to the grid's structure and minimize the number of off-slice cache accesses
<code>setNElements</code>	int n, int accID	To communicates to each SPU how many elements to compute. All the SPUs maintain a counter to keep track of their progress and stop when the desired number of elements has been computed
<code>startAccelerator</code>	-	The final function starts with the execution of all the plSPU

and one output stream to store the result (line 26). As the elements $A[j][i-1]$, $A[j][i]$, and $A[j][i+1]$ are laid out in consecutive memory addresses, we can reuse the same stream and leverage the support for unaligned loads by shifting the access to the left (right) by one element to load the data. Finally, the number of elements to compute for each SPU (line 28) is configured, and the computation starts (line 30).

Figure 7 shows the stencil instructions executed on the SPU. As the stencil loads data from five input points, the instruction sequence consists of five instructions. All the input points are multiplied by the constant 0.2. This means all the instructions encode the same constant factor $c0$. The instructions load data from three different streams: the first stream points to the value $A[j-1][i]$, aligned to a cache line boundary. The values $A[j][i-1]$, $A[j][i]$, and $A[j][i+1]$ are stored in consecutive memory addresses. These three accesses all use the same stream, but using a shift amount and direction included in the request for the elements at indices $i+1$ and $i-1$. This loads the correctly aligned data using the unaligned load mechanism. Finally, the third stream is configured to load the value at $A[j+1][i]$.

```

1  // 0.2 * A[j-1][i]
2  c0, s1, 0, 0, 1, 0, 1 //no shift, clear acc, inc stream
3  // 0.2 * A[j][i-1]
4  c0, s2, 1, 0, 0, 0, 0 //shift right by 1
5  // 0.2 * A[j][i]
6  c0, s2, 0, 0, 0, 0, 0 //no shift
7  // 0.2 * A[j][i+1]
8  c0, s2, 0, 1, 0, 0, 1 //shift left, inc stream
9  // 0.2 * A[j+1][i]
10 c0, s3, 0, 0, 1, 1 //enable output, inc stream

```

Figure 7: Instruction sequence for the Jacobi-2D stencil.

The final 3 bits of each instruction hold control information for the SPU. For example, the first bit clears the accumulator before the accumulation step. This bit must be set by the first instruction of a grid point (line 2). The next bit enables the output. It is set in the last instruction of the sequence (line 10) and generates a store request. The final bit signals the SPU to advance the stream. It has to be set in the last instruction consuming data from each stream (lines 2, 8, 10).

7 METHODOLOGY

7.1 Experimental Setup

We simulate the performance of Casper using the gem5 simulator in syscall emulation mode [7]. Table 2 describes our system configuration in details. We use the ARM ISA and the Ruby memory

model. The system is based on a generic modern server-class CPU, consisting of 16 out-of-order cores and three levels of cache, having a sliced LLC with 2MB per slice. Our baseline configuration uses the same system configuration without the plSPU and the LLC changes we propose. Also, we include stride prefetchers at all levels of the cache hierarchy. We evaluate the performance and energy benefit of Casper against the baseline CPU architecture, an NVIDIA Titan V GPU[27]. We use an energy model based on CACTI 7.0 [5] and energy models proposed by prior works [42, 43]. We use the area model presented in [35] scaled down to 22nm to estimate the area of the SPU. For the GPU performance/area comparisons, we use the complete die size of 815mm² of the Titan V [28] because typical GPU-accelerated systems also need a host CPU to perform the computation. As a result, the total area for the end-user is either the complete GPU or the Casper hardware modifications, added to the area of the existing host CPU.

Table 2: Simulation Parameters

Component	Configuration
<i>Casper</i>	16 plSPU, 1 SIMD unit/SPU (512bits wide)
<i>Core</i>	10 entry load queue, 0.016 nJ/instruction 16 out-of-order cores, 2 GHz, 8-wide issue, 72 entry load queue, 64 entry store queue, 1 SIMD unit/core (512bits wide)
<i>L1/L2 Cache</i>	224 entry ROB, 0.08nJ per instruction 32kB, private, 8-way, 16 MSHRs, 4 cycle round-trip latency, 2 load ports, 1 store port 15/33 pJ per hit/miss [43]
<i>L2 Cache</i>	256kB, private, 8-way, 16 MSHRs, 12 cycle round-trip latency, 1 load port, 1 store port 46/93 pJ per hit/miss [43]
<i>L3 Cache</i>	32MB, shared, 16-way, 16 slices, 32 MSHRs/slice 36 cycle round-trip latency, 1 load/store port per slice 945/1904 pJ per hit/miss [43]
<i>Coherence Protocol</i>	MESI
<i>Replacement Policy</i>	LRU replacement
<i>Hardware Prefetchers</i>	Stride prefetchers at all levels of the cache
<i>On-Chip Network</i>	mesh, XY-routing, 64B/cycle per direction
<i>Main Memory</i>	16GB, DDR4, 4 channels, 160nJ per read/write [42]

7.2 Benchmarks

We evaluate Casper on six stencil benchmarks, including up to 3-dimensional stencils with varying data reuse characteristics, ranging from 3 input points (Jacobi 1D) up to 33 points for the 33-point 3D stencil. We use Jacobi 1D, -2D, 7-point 3D (heat diffusion) from

Polybench [31], a 5×5 Gaussian blur filter [8], the 7-point 1D kernel from [19], and a 33-point 3D kernel to represent higher-order scientific simulations [12, 13]. All the benchmarks use Jacobi-style stencils with disjoint read and write data sets. The benchmarks are elementary stencils that can be conjugated to form more complex stencils occurring in real-world applications. In addition to the standard data set sizes (which fit inside the LLC of the CPU), we also evaluate Casper on data sets that 1) exceed the size of the LLC (named *DRAM*), and 2) fit within the private L2 caches of the CPU (*L2*). Table 3 lists the domain sizes. We report the runtime for one timestep ($T = 1$ in Figure 2), measured at the third timestep of the benchmarks. Iteration runtimes are stable, starting from the third timestep in our benchmarks. Because of T is usually large enough to amortize the cost of moving the data from memory, we do not consider this in the evaluations.

Table 3: Domain size used for evaluations

Level	1D	2D	3D
<i>L2</i>	131,072	512×256	$64 \times 64 \times 32$
<i>L3</i>	1,048,576	1024×1024	$128 \times 128 \times 64$
<i>DRAM</i>	4,194,304	2048×2048	$256 \times 256 \times 64$

8 RESULTS

8.1 Performance

Figure 8 shows the speedup of Casper compared to a 16-core baseline system. For the datasets that fit within the LLC, which represent typical data set sizes for stencil computations, we observe an average speedup of $1.65 \times$. The 1- and 2-dimensional stencils achieve speedups between $1.66 \times$ and $3.0 \times$. However, the 3-dimensional stencils cannot achieve the same performance and even experience a slowdown in the 33-point stencil case. The reason for this performance is twofold. First, the 3-dimensional stencils need to load a significant part of their input data from remote LLC slices, which introduces longer access latencies and lowers the throughput of the plSPU. Second, the 33-point 3D stencil has good L1 cache behavior in the baseline, achieving a hit-rate of 95%. Thus, this stencil is well-suited for execution on a traditional CPU with regards to performance. We conclude that the performance benefits of Casper are larger on lower-dimensional stencils that load most of their input data from the local LLC slice.

The average performance improvement for the smaller data set that fits within the L2 caches of the CPU is $1.89 \times$. Even though the data is stored closer to the core and does not need to travel through the entire cache hierarchy, the speedups are similar to the larger data sets that fit within the LLC. This is the case because the access latency from the CPU to the L2 cache is similar to the latency between SPU and the closest LLC slice (12 vs 8 cycles load-to-use). The 3-dimensional benchmarks even reach better performance improvements than on larger datasets. This is the case because the baseline performance is limited by cache lines ping-ponging between private caches via the LLC. Casper avoids this problem by computing directly on the shared LLC.

Our results show that for large data sets that exceed the size of the LLC, Casper improves performance by $1.4 \times$, on average. The highest speedups are achieved by the 2-dimensional stencils, with *Blur 2D* reaching $4.16 \times$. We explain this by the fact that the baseline

has a very low LLC hit-rate (only 2%), and thus the number of memory accesses is $4 \times$ higher than in Casper. The main reason for this low hit-rate is that the prefetchers are interfering with demand accesses, evicting cache lines out of the LLC before they are used. The remaining stencils perform similar to the baseline or even experience slowdowns. The reason for this is the fact that memory bandwidth is the main bottleneck. The 33-point 3D stencil again experiences a slowdown because it is well-suited for computation with smaller private caches for each core. We conclude that even though Casper cannot alleviate the memory bandwidth bottleneck for large data sets, it does not lead to significant slowdowns for most stencils.

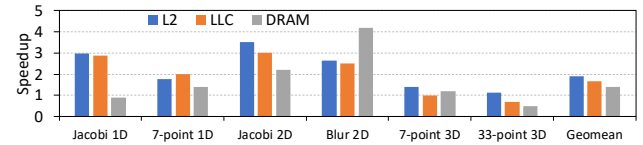


Figure 8: Speedup compared to the baseline multi-core system.

8.2 Energy Consumption

Figure 9 shows the normalized energy consumption of Casper compared to the baseline CPU. For the data sets that fit into the LLC, Casper reduces energy consumption by 55%, on average. Casper reduces energy consumption by 49% even for the 33-point 3D stencil, whose performance is slower in Casper than in the baseline. The reduction in energy consumption is higher for simpler stencils (Jacobi 1D/2D, 7-point 3D), reaching up to as 65% for 7-point 3D. The reason for this is that more complex stencils perform more LLC accesses and since the plSPU are situated close to the LLC slice, accessing the LLC is not as energy-efficient as accessing the smaller L1 cache. This results in lower energy savings for the more complex stencils because of higher L1 reuse in baseline CPUs.

For the smaller and larger data sets, Casper reduces energy consumption by to 26% and 23%, on average respectively. We make two observations: First, Casper increases the energy consumption of the 1-dimensional benchmarks (Jacobi 1D and 7-point 1D) when compared to the baseline, for both small and large data sets. For the large data sets, this is the case because the CPU cores can be idle for most of the runtime, waiting for memory. For the smaller data set, the baseline's energy consumption is very low because there are very few LLC accesses. Since Casper loads the data from the shared LLC, it increases energy consumption in such cases. Second, for all the other benchmarks, Casper reduces energy consumption significantly. Casper is more energy-efficient even for the benchmarks that the CPU baseline outperforms since our SPU design is more energy-efficient than the CPU baseline. Thus, we conclude that Casper achieves significant reductions in energy consumption compared to an out-of-order CPU.

8.3 Comparison with GPU

Figure 10 shows Casper's performance and performance-per-area normalized to an NVIDIA Titan V GPU. GPU outperforms Casper by $3.71 \times$, $2.89 \times$, and $36.64 \times$ on average across all stencils that fit inside L2, LLC, and DRAM respectively. However, in all stencil kernels

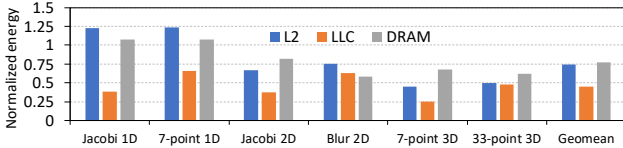


Figure 9: Normalized energy consumption compared to the 16-core baseline.

Casper provides higher performance-per-area, up to 190 \times compared to GPU. We observe that the L2- and LLC-sized data sets achieve performance-per-area improvements of 47 \times and 60 \times , respectively. For these data set sizes, Casper has the advantage of its tight integration into the large LLC. At the same time, the data does not fit into the GPU caches. For the large DRAM-sized data sets, however, the average improvement in performance/area is only 4.78 \times . In this case, GPU improves relative performance because of its higher memory bandwidth.

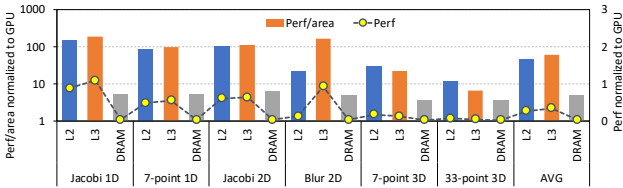


Figure 10: Performance/area compared to an NVIDIA Titan V GPU for three different domain sizes.

8.4 Effect of Individual Optimizations

The SPUs in Casper take advantage of two key optimizations: 1) a custom *data mapping* in LLC, which creates stencil segments to maximize the accesses of an SPU to the own LLC slice, and 2) the *near-cache* (near-LLC) location of the SPUs, which minimizes data access latency and leverages the peak bandwidth of the LLC. In this section, we evaluate the contribution of each optimization to the overall performance. The baseline for this analysis is a system where the SPUs are located next to the private L1 caches of CPU cores. The baseline LLC data mapping places consecutive cache lines in consecutive LLC slices (similar to [47]). First, we apply the data mapping optimization and compare the performance to the baseline. Second, we apply both the data mapping optimization and the near-cache optimization.

We make two observations from the results in Figure 11. First, computing near-cache (green portion of the bars) is the major contributor to the speedup. Second, the custom data mapping (blue portion of the bars) produces up to 30% of the speedup (Jacobi 1D with LLC data set), but its effect is negligible (or even negative) in several cases (1D and 2D benchmarks with L2/DRAM data sets, 7-point 3D with LLC data set). In these cases, the custom data mapping results in a number of accesses to remote LLC slices which is similar to the baseline data mapping.

8.5 Hardware Cost

Stencil Processing Unit. The area of one SPU scaled to 22nm technology is 0.146 mm². The most significant contributors to this area are the execution unit and the SRAM array used to buffer complete memory requests.

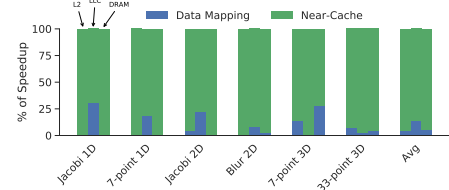


Figure 11: Contribution of custom data mapping and near-cache SPU location to the speedup of Casper over a baseline system with SPUs near L1 for L2-/LLC-/DRAM-sized data sets.

Unaligned Loads. Our hardware mechanism to support unaligned loads consumes an additional 0.14 mm² compared to the baseline 2MB SRAM cache slice. This amounts to a 5% increase in area per LLC slice. Almost the complete area overhead is attributed to the second read port of the tag array, which consumes 0.12 mm² of space. The remaining hardware overhead of one 3:1 multiplexer per SRAM row, the barrel shifter to rotate the final output, and the split multiplexers for way selection are minimal compared to the tag array overhead.

Address to LLC slice mapping. Identifying the stencil segment needs two registers to store the start and the length of the segment. The comparison needs one adder and one comparator. The new mapping is a simple bit-select from the physical address, and thus requires minimal additions. This hardware is introduced at every NoC injection point.

In summary, the hardware additions proposed in this paper require an additional 4.65 mm² of die area for a system using 16 SPUs. This amounts to a 0.77% area increase compared to the Marvell ThunderX 2 CPU [24], a server-class ARM CPU implemented in 16nm hosting 32MB of LLC.

9 RELATED WORK

To the best of our knowledge, we present the first work that tightly integrates specialized compute units into the last-level cache of a CPU to perform stencil computations. In this section, we succinctly compare prior proposals against Casper.

A wide body of research has focused on studying and analyzing stencil computations [3, 16, 18, 22, 26, 32, 38]. PIMS [22] is the most closely-related work to Casper. PIMS exploits high-bandwidth provided by 3D-stacking (e.g., HMC, HBM) to accelerate stencils. Casper, being a near-LLC accelerator, can be integrated with any commodity processor without the need of costly interfacing using through-silicon vias. Szustak et al. [39] accelerate the MPDATA stencil kernel on multi-core CPU while Thaler et al. [41] port weather stencil kernels to a many-core system. GPUs [2, 16] have been shown to increase performance due to the high degree of parallelism present in the computation. Wahib et al. [45] develop an analytical performance model for choosing an optimal GPU-based execution strategy for various scientific stencil kernels. Gysi et al. [18] provide guidelines for optimizing stencil kernels for CPU-GPU systems.

More recently, the use of FPGAs to accelerate stencils has been proposed [9, 36, 37, 44]. Augmenting general-purpose cores with specialized FPGA accelerators is a promising approach to enhance overall system performance. However, data still needs to be moved

to these off-chip external accelerators. Moreover, taking full advantage of FPGAs for accelerating a workload is not a trivial task as it requires sufficient FPGA programming skills to map the workload and optimize the design for the FPGA microarchitecture. In contrast, processing close to memory tightly integrates compute units close to the memory. This integration avoids unnecessary data-movement.

10 CONCLUSION

We present Casper, a novel near-cache acceleration system for stencil computations. Our throughput-optimized stencil processing units and their placement near the LLC enable a high performance and energy-efficient execution for stencil computations. The design performs stencil computations close to where data resides and orchestrates data accesses to minimize data movements. With the addition of hardware support to map consecutive blocks of data to the same LLC slice and by exploiting the memory level parallelism, we reach our goal to match the system's compute potential to the bandwidth offered by the LLC with an area overhead of less than 1%. Our evaluations show that Casper improves performance by 65% on typical data sets used for stencil computations. Compared to a state-of-the-art GPU, performance per area improves on average by 37 \times . Across all our benchmarks, Casper reduces energy consumption by 35% compared to the CPU baseline.

REFERENCES

- [1] J. Ahn, S. Yoo, O. Mutlu, and K. Choi, "PIM-enabled instructions: a low-overhead, locality-aware processing-in-memory architecture," in *ISCA*, 2015.
- [2] O. Arjum, S. Garcia de Gonzalo, M. Hidayetoglu, and W.-M. Hwu, "An Efficient GPU Implementation Technique for Higher-Order 3D Stencils," in *HPCC*, 2019.
- [3] A. Armejach, H. Caminal, J. M. Cebrian, R. González-Alberquilla, C. Adeniyi-Jones, M. Valero, M. Casas, and M. Moretó, "Stencil codes on a vector length agnostic architecture," in *PACT*, 2018.
- [4] W. Augustin, V. Heuveline, and J.-P. Weiss, "Optimized stencil computation using in-place calculation on modern multicore systems," in *ECPP*, 2009.
- [5] R. Balasubramonian, A. B. Kahng, N. Muralimanohar, A. Shafiee, and V. Srinivas, "CACTI 7: New tools for interconnect exploration in innovative off-chip memories," *TACO*, 2017.
- [6] A. Basu, J. Gandhi, J. Chang, M. D. Hill, and M. M. Swift, "Efficient virtual memory for big memory servers," in *ISCA*, 2013.
- [7] N. Binkert, B. Beckmann, G. Black, S. K. Reinhardt, A. Saidi, A. Basu, J. Hestness, D. R. Hower, T. Krishna, S. Sardashti *et al.*, "The gem5 simulator," *ACM SIGARCH Computer Architecture News*, 2011.
- [8] J. Cann, "A computational approach to edge detection," *IEEE Transactions on pattern analysis and machine intelligence*, 1986.
- [9] Y. Chi, J. Cong, P. Wei, and P. Zhou, "SODA: Stencil with Optimized Dataflow Architecture," in *ICCAD*, 2018.
- [10] M. Christen, O. Schenk, and Y. Cui, "Patus for convenient high-performance stencils: evaluation in earthquake simulations," in *SC*, 2012.
- [11] P. Colella, "Defining software requirements for scientific computing," 2004.
- [12] K. Datta, M. Murphy, V. Volkov, S. Williams, J. Carter, L. Oliker, D. Patterson, J. Shalf, and K. Yelick, "Stencil computation optimization and auto-tuning on state-of-the-art multicore architectures," in *SC*, 2008.
- [13] K. Datta and K. A. Yelick, *Auto-tuning stencil codes for cache-based multicore platforms*. University of California, Berkeley, 2009.
- [14] J. W. Demmel, *Applied numerical linear algebra*. SIAM, 1997.
- [15] C. Eckert, X. Wang, J. Wang, A. Subramaniyan, R. Iyer, D. Sylvester, D. Blaauw, and R. Das, "Neural cache: Bit-serial in-cache acceleration of deep neural networks," in *ISCA*, 2018.
- [16] O. Fuhrer, T. Chadha, T. Hoefer, G. Kwasniewski, X. Lapillonne, D. Leutwyler, D. Lüthi, C. Osuna, C. Schär, T. C. Schulthess *et al.*, "Near-global climate simulation at 1 km resolution: establishing a performance baseline on 4888 GPUs with COSMO 5.0," *Geoscientific Model Development*, 2018.
- [17] O. Fuhrer, C. Osuna, X. Lapillonne, T. Gysi, M. Bianco, and T. Schulthess, "Towards gpu-accelerated operational weather forecasting," in *The GPU Technology Conference*, 2013.
- [18] T. Gysi, T. Grosser, and T. Hoefer, "Modesto: Data-centric analytic optimization of complex stencil programs on heterogeneous architectures," in *SC*, 2015.
- [19] J. Holewinski, L.-N. Pouchet, and P. Sadayappan, "High-performance code generation for stencil computations on GPU architectures," in *SC*, 2012.
- [20] M. Imani, S. Gupta, Y. Kim, and T. Rosing, "FloatPIM: In-memory Acceleration of Deep Neural Network Training with High Precision," in *ISCA*, 2019.
- [21] N. P. Jouppi, "Improving Direct-Mapped Cache Performance by the Addition of a Small Fully-Associative Cache and Prefetch Buffers," in *ISCA*, 1990.
- [22] J. Li, X. Wang, A. Tumeo, B. Williams, J. D. Leidel, and Y. Chen, "PIMS: a lightweight processing-in-memory accelerator for stencil computations," in *ISMS*, 2019.
- [23] N. Maruyama and T. Aoki, "Optimizing stencil computations for nvidia kepler gpus," in *Proceedings of the 1st international workshop on high-performance stencil computations*, Vienna, 2014, pp. 89–95.
- [24] Marvell, "ThunderX2 CPU." [Online]. Available: <https://en.wikichip.org/wiki/cavium/thunderx2>
- [25] G. A. McMechan, "Migration by extrapolation of time-dependent boundary values," *Geophysical Prospecting*, vol. 31, no. 3, pp. 413–420, 1983.
- [26] A. Nguyen, N. Satish, J. Chhugani, C. Kim, and P. Dubey, "3.5-D blocking optimization for stencil computations on modern CPUs and GPUs," in *SC*, 2010.
- [27] Nvidia, "NVIDIA TITAN V." [Online]. Available: <https://www.nvidia.com/en-us/titan/titan-v/>
- [28] Nvidia, "The nvidia titan v preview," Dec 2017. [Online]. Available: <https://www.anandtech.com/show/12170/nvidia-titan-v-preview-titanomachy>
- [29] C. Olschanowsky, M. M. Strout, S. Guzik, J. Loffeld, and J. Hittinger, "A study on balancing parallelism, data locality, and recompilation in existing PDE solvers," in *SC*, 2014.
- [30] E. H. Phillips and M. Fatica, "Implementing the Himeno benchmark with CUDA on GPU clusters," in *IPDPS*, 2010.
- [31] L.-N. Pouchet, "Polybench: The polyhedral benchmark suite," URL: <http://www.cs.ucla.edu/pouchet/software/polybench>, 2012.
- [32] J. Ragan-Kelley, C. Barnes, A. Adams, S. Paris, F. Durand, and S. Amarasinghe, "Halide: a language and compiler for optimizing parallelism, locality, and recompilation in image processing pipelines," in *PLDI*, 2013.
- [33] K. Sano, Y. Hatsuda, and S. Yamamoto, "Multi-FPGA accelerator for scalable stencil computation with constant memory bandwidth," *TPDS*, 2013.
- [34] V. Seshadri, D. Lee, T. Mullins, H. Hassan, A. Boroumand, J. Kim, M. A. Kozuch, O. Mutlu, P. B. Gibbons, and T. C. Mowry, "Ambit: In-memory accelerator for bulk bitwise operations using commodity DRAM technology," in *MICRO*, 2017.
- [35] Y. S. Shao, B. Reagen, G.-Y. Wei, and D. Brooks, "Aladdin: A pre-rtl, power-performance accelerator simulator enabling large design space exploration of customized architectures," in *ISCA*, 2014.
- [36] G. Singh, D. Diamantopoulos, C. Hagleitner, J. Gómez-Luna, S. Stuijk, O. Mutlu, and H. Corporaal, "NERO: A Near High-Bandwidth Memory Stencil Accelerator for Weather Prediction Modeling," in *FPL*, 2020.
- [37] G. Singh, D. Diamantopoulos, C. Hagleitner, S. Stuijk, and H. Corporaal, "NARMADA: Near-Memory Horizontal Diffusion Accelerator for Scalable Stencil Computations," in *FPL*, 2019.
- [38] H. Stengel, J. Treibig, G. Hager, and G. Wellein, "Quantifying performance bottlenecks of stencil computations using the execution-cache-memory model," in *ICS*, 2015.
- [39] L. Szustak, K. Rojek, and P. Gepner, "Using Intel Xeon Phi Coprocessor to Accelerate Computations in MPDATA Algorithm," in *PPAM*, 2013.
- [40] A. Taflove, "Review of the formulation and applications of the finite-difference time-domain method for numerical modeling of electromagnetic wave interactions with arbitrary structures," *Wave Motion*, 1988.
- [41] F. Thaler, S. Moosbrugger, C. Osuna, M. Bianco, H. Vogt, A. Afanasyev, L. Mosimann, O. Fuhrer, T. C. Schulthess, and T. Hoefer, "Porting the COSMO Weather Model to Manycore CPUs," in *PASC*, 2019.
- [42] P.-A. Tsai, N. Beckmann, and D. Sanchez, "Jenga: Software-defined cache hierarchies," in *ISCA*, 2017.
- [43] P.-A. Tsai, C. Chen, and D. Sanchez, "Adaptive scheduling for systems with asymmetric memory hierarchies," in *MICRO*, 2018.
- [44] J. van Lunteren, R. Luijten, D. Diamantopoulos, F. Auernhammer, C. Hagleitner, L. Chelini, S. Corda, and G. Singh, "Coherently Attached Programmable Near-Memory Acceleration Platform and its application to Stencil Processing," in *DATE*, 2019.
- [45] M. Wahib and N. Maruyama, "Scalable Kernel Fusion for Memory-Bound GPU Applications," in *SC*, 2014.
- [46] S. Williams, A. Waterman, and D. Patterson, "Roofline: an insightful visual performance model for multicore architectures," *Communications of the ACM*, vol. 52, no. 4, pp. 65–76, 2009.
- [47] Y. Yarom, Q. Ge, F. Liu, R. B. Lee, and G. Heiser, "Mapping the intel last-level cache." *IACR Cryptology ePrint Archive*, vol. 2015, p. 905, 2015.